Selective transformation of biomass-derived 5-hydroxymethylfurfural to the building blocks 2,5-bis(hydroxymethyl)furan on α-Ni(OH)$_2$/SiO$_2$ catalyst without prereduction

Weixing Pan[1] · Hui Chen[1] · Aicheng Chen[1]

Abstract

A series of low-cost α-Ni(OH)$_2$/SiO$_2$ catalysts were successfully fabricated by the vapor-induced internal hydrolysis method, then the hydrogenation of 5-hydroxymethylfurfural (HMF) to 2,5-bis(hydroxymethyl)furan (BHMF) was investigated by using the ethanol as the hydrogen donor over these as-prepared α-Ni(OH)$_2$/SiO$_2$ catalysts. Based on the reaction results, these as-prepared catalysts, which could dispense with extra pre-reduction treatment before reactions, exhibited superior catalytic performance for the HMF hydrogenation to BHMF. A remarkable intrinsic selectivity of BHMF selectivity of almost 100% with about 90% HMF conversion could be obtained under 195 °C for 5 h in an N$_2$ atmosphere over the α-Ni(OH)$_2$/SiO$_2$ catalyst of 5-Ni(OH)$_2$/SiO$_2$ with about 5 wt% Ni on SiO$_2$. The almost constant HMF conversion and BHMF intrinsic selectivity found from the recycling tests can indicate that the catalyst was stable without the obvious loss of its catalytic activity after recycling. Moreover, the mechanism of HMF hydrogenation using ethanol over the α-Ni(OH)$_2$/SiO$_2$ catalysts could be referred to as the mechanism of the Meerwein-Ponndorf-Verley reaction. This work will provide a simple synthesis method for future design and development of high-performance, low-cost, and low-energy consumption catalysts for HMF hydrogenation to BHMF.

✉ Aicheng Chen
chenaicheng@fjnu.edu.cn

1   Fujian Provincial University Engineering Research Center of Industrial Biocatalysis, College of Chemistry and Materials Science, Fujian Normal University, Fuzhou 350007, People's Republic of China

Introduction

The biomass platform molecule 5-hydroxymethylfurfural (HMF) has been regarded as the key bridge connecting petroleum-based and biomass resources. Now, many oxidative and reductive derivatives of HMF have displayed great potential as a sustainable substitute for petroleum-derived chemicals [1–3]. Among these derivatives, a renewable high value-added diol of 2,5-bis(hydroxymethyl)furan (BHMF) has attracted significant attention and been widely applied in the synthesis of fine chemicals and artificial receptors, like pharmaceuticals, ethers, ketones, artificial fibers, resins, and so on [1, 4]. Furthermore, the etherification products of BHMF formed with alcohols were also value-added chemicals as potential bio-diesel candidates [5, 6]. Therefore, the selective reduction of HMF to BHMF understandably has received much attention recently.

BHMF is a chemical intermediate during the preparation of other further value-addition hydrogenated furanic derivatives starting from HMF. It will be readily further reduced to 5-methylfurfuryl alcohol (MFA), 2,5-bis(hydroxymethyl)tetrahydrofuran (BHMTHF), 2,5-dimethylfuran (DMF), and other chemicals [1, 3, 7]. Then, the efficient selective hydrogenation of HMF to BHMF is still a challenge. Recently, many metal-based catalysts have been employed for the selective reduction of HMF to BHMF, such as Au, Co, Cu, Hf, Ir, Ni, Pd, Pt, Re, Ru, and so on [7]. To obtain outstanding performance, these above-mentioned catalysts generally would be pre-reduced by H_2 at a high temperature [8] or sodium borohydride [9] and hydrazine monohydrate [10] at room temperature. This treatment is clearly not green enough. To overwhelm this drawback, some catalysts (like Ru and Ir pincer complexes [11], $ZrO(OH)_2$ [12], and MOF-based catalysts [3]) without pre-reduction were been designed for HMF reduction to BHMF in recent years. However, these non-pre-reduction catalysts are mostly not the "supported catalysts ", then the usage and cost of active components in them will become another drawback for their industrialized applications. Besides catalysts, the hydrogen donors also play a crucial role during the HMF hydrogenation. Generally, H_2, alcohols, and formic acid were often regarded as the candidates for the hydrogen donor in the HMF hydrogenation. Thereinto, H_2 dominantly comes from petroleum cracking and can't be effectively utilized for the low solubility in the solvent during the HMF hydrogenation. This hurts the sustainable development of world energy, though the catalyst usually displays a good performance under the H_2 atmosphere. Formic acid (FA) can be obtained from biomass resources [13] and is regarded as a promising hydrogen storage compound [14], but it might undermine the activity and stability of the catalyst for its acidity and corrosivity to some content. So, the more convenient and safe hydrogen sources of alcohols [1] might be considered as a suitable hydrogen donor for HMF to BHMF. Considering the oil crisis and environmentally sustainable development, it is essential to develop a non-precious supported catalyst without pre-reduction for the HMF hydrogenation to BHMF by alcohols.

Hence, in the present work, a kind of α-Ni(OH)$_2$/SiO$_2$ supported catalyst was prepared by the vapor-induced internal hydrolysis (VIH) method [15], and then

the selective transformation of biomass-derived HMF to the renewable high value-added building blocks of BHMF was performed by using the ethanol as the hydrogen donor over these as-prepared catalysts without pre-reduction.

Experimental

Material

The support of SiO_2 was supplied by Xinchanglai Silicone Co. Ltd. (Qingdao, China). $Ni(NO_3)_2 \cdot 6H_2O$ ($\geq 98\%$) was provided by Xilong Chemical Co. Ltd. (Shenyang, China). Aqueous ammonia (25–28%) was obtained from Sinopharm Chemical Reagent Co. Ltd. (Shanghai, China). Ethanol ($\geq 99.7\%$) was purchased from Zesheng Technology Co. Ltd. (Anhui, China). 5-hydroxymethylfurfural (HMF, 99%), 2,5-dihydroxymethylfuran (BHMF, 98%), and acetonitrile ($\geq 99.9\%$) were supplied by Aladdin Reagents Co. Ltd. (Shanghai, China).

Catalyst preparation

The transition metal nickel was introduced to the SiO_2 support by incipient wetness impregnation. Thereinto, the typical nickel precursor of hydrous nickel nitrate ($Ni(NO_3)_2 \cdot 6H_2O$) 0.25 g was dissolved with 1.40 g of H_2O and then loaded on 1.00 g of the SiO_2 support. After that, the sample was held at room temperature for 12 h and then heated at 120 °C for 4 h. Subsequently, 0.20 g of the as-prepared samples were treated with 5 mL ammonia solution by the VIH method [15] at 60 °C for 3 h in a 100 mL autoclave (Fig. S1). Herein, the ammonia used during the VIH process was controlled according to the required amount for converting Ni^{2+} to $Ni(OH)_2$ on the catalysts. At last, the samples were heated 205 °C for 6 h to acquire the α-$Ni(OH)_2/SiO_2$ catalyst. The as-prepared α-$Ni(OH)_2/SiO_2$ catalyst was named x-$Ni(OH)_2/SiO_2$, where x denotes the Ni content in the catalysts.

Catalyst characterization

X-ray powder diffraction (XRD) patterns were recorded on a Rigaku Ultima IV X-ray diffractometer with Cu K_α radiation (0.154 nm) with a scanning rate of 10° min^{-1} in the range of $2\theta = 10$–80°.

N_2 isotherms were measured on a Micrometritics ASAP 2460 M instrument at -196 °C. Before testing, the samples were pretreated at 80 °C for 6 h under vacuum. The specific surface areas of the catalysts were measured by the Brunauer–Emmett–Teller (BET) method, and the pore-size distribution and total pore volume were obtained by the Barrett-Joyner-Halenda (BJH) method.

X-ray photoelectron spectroscopy (XPS) spectra of Ni 2p levels of the investigated catalysts were recorded on a Thermo Fisher Scientific K-Alpha spectrometer by using monochromatic Al Kα radiation ($hv = 1486.6$ eV). The binding energy (BE) scale was calibrated to the C 1s peak at 284.8 eV.

The H_2 temperature programmed reduction (H_2-TPR) was performed on a Chemisorb 2720 instrument (Micrometritics Instrument Corp., USA) with a heating rate of 10 °C min^{-1} in the temperature ramp from room temperature to 900 °C. Before measuring, about 50 mg sample was pretreated at 120 °C for 1 h with Ar. After that, the H_2-TPR test would be launched with the carrier gas of 10% H_2 in Ar. The exhaust gas from the sample cell would pass through a cold trap to remove H_2O created during the metal reduction, before entering the thermal conductivity detector. The cold trap was prepared by a mixture of isopropyl alcohol and liquid nitrogen.

Infrared (IR) absorption spectra were recorded using a Thermo Fisher Scientific Nicolet Is50 FT-IR spectrometer. Because KBr can react with layered hydroxide phases [16], cesium iodide (CsI) optics were used for the measurement in this work.

The High-resolution transmission electron microscopy (HRTEM) was conducted on an FEI Talos-F200s microscope at an accelerating voltage of 200 kV. Before the HRTEM test, the samples were ultrasonically dispersed using ethanol and then supported on a copper mesh. Moreover, the actual Ni content in catalysts was measured by inductively coupled plasma optical emission spectroscopy (ICP-OES) on an Agilent 720 ICP-OES spectrometer.

Reaction procedure and product analysis

The hydrogenation of HMF was carried out in a YZQR-50 reactor (YanZheng Instrument Equipment Co. Ltd). Typically, 0.50 mmol HMF was dissolved in 30 mL EtOH, and then the catalyst was added into the as-prepared HMF alcoholic solution. The dosage of the catalyst was according to the molar ratio of n_{Ni}: $n_{HMF} = 1:10$ in the reaction solution. Next, the mixture was placed into a 50 mL polytetrafluoroethylene container and then put into the reactor with magnetic stirring, and replacing the gas in the reactor with molecular nitrogen three times. Then 0.2 MPa of nitrogen would be kept in the reactor before the reaction began. After that, the reaction temperature was raised, and the HMF hydrogenation started. After the reaction temperature up to 195 °C, the pressure of the reactor was increased to about 2.5 MPa.

After the HMF hydrogenation, the reaction mixture was analyzed on a Shimadzu LC-16P high-performance liquid chromatography (HPLC). The products of HMF and BHMF were separated from the initial product using a ZORBAX SBAq C18 column (4.6×250 mm, 5 μm, Agilent, USA). The mobile phase is a mixture of acetonitrile and 0.1 wt% trifluoroacetic acid in water with a volume ratio of 5: 95 at 30 °C (0.5 mL min^{-1}). Before the analysis, the reaction mixture was filtered with 0.22 μm polytetrafluoroethylene filters. The content of HMF and BHMF was quantified by an external calibration curve method on basis of HPLC analysis, and the 5-(ethoxymethyl)furfural alcohol (EMFA) and 2,5-bis(ethoxymethyl)furfural (BEMF) were identified by a GC9790II gas chromatography (Fuli Analytical Instruments Corp., China) using an HP-5 column (30 m×0.32 mm, 0.25 μm). Then the HMF conversion and product selectivity were calculated.

Results and discussion

Characterization of catalysts

As shown in the XRD patterns in Fig. 1a, the diffraction peaks of 2θ at 12.8°, 33.1°, 35.5°, 58.9°, and 60.5° can be assigned to the (001), (100), (101), (110), and (111) lattice planes according to the standard pattern (JCPDS No. 22-0752) for nickel nitrate hydroxide. Generally, the "α-Ni(OH)$_2$ " often contains intercalated anions and water molecules for its hydroxyl-deficient phase [17, 18]. So, the general formula of α-Ni(OH)$_2$, can be written as [Ni(OH)$_{2-x}$A$_x$/$_n^{n-}$ ·yH$_2$O] with $x = 0.2$–0.4, $y = 0.6$–1, and A = Cl$^-$, NO$_3^-$, SO$_4^{2-}$, CO$_3^{2-}$, or OCN$^-$ [17, 18]. Thus, based on the general formula of α-Ni(OH)$_2$ and no visible peaks from β-Ni(OH)$_2$ and NiO in the XRD pattern, the Ni(OH)$_2$ on the catalysts in this study was definitely the α-form. Moreover, there are some major characteristics of α-Ni(OH)$_2$ proposed in previous reports [19] can also be found in Fig. 1a. In detail, α-Ni(OH)$_2$ often has the strongest XRD diffraction peak around $2\theta = 12$°, an asymmetric broad peak at about 32~35°, and none of the general reflection for the brucite structure [19]. Moreover, as shown in the HRTEM image of 5-Ni(OH)$_2$/SiO$_2$ in Fig. 1b, the quantified interlayer spacing of 0.27 nm and 0.25 nm were attributed to the (100) and (101) crystal facets for α-Ni(OH)$_2$, respectively. Given the above-mentioned, Ni species in the as-prepared catalysts were in the form of α-Ni(OH)$_2$. In addition, when the content of Ni in the catalyst was below 5% on the catalysts of 1-Ni(OH)$_2$/SiO$_2$, 2-Ni(OH)$_2$/SiO$_2$, and 5-Ni(OH)$_2$/SiO$_2$, non-obvious diffraction peaks attributed to α-Ni(OH)$_2$ revealed that α-Ni(OH)$_2$ was highly dispersed on the catalysts or too small crystal particles formed to be detected by XRD.

Moreover, a shoulder peak at about 3633 cm^{-1} from the IR spectra in Fig. 2 could be attributed to the interlayer H$_2$O from α-Ni(OH)$_2$ [20], and O–H bend of lattice OH from α-Ni(OH) and lattice mode for α-Ni(OH)$_2$ could be found at the peaks of about 1409 cm^{-1} and about 682 cm^{-1} [20, 21]. These would suggest that the synthesized Ni(OH)$_2$ was the α-phase form. In addition, the peaks at 3438 cm^{-1} and
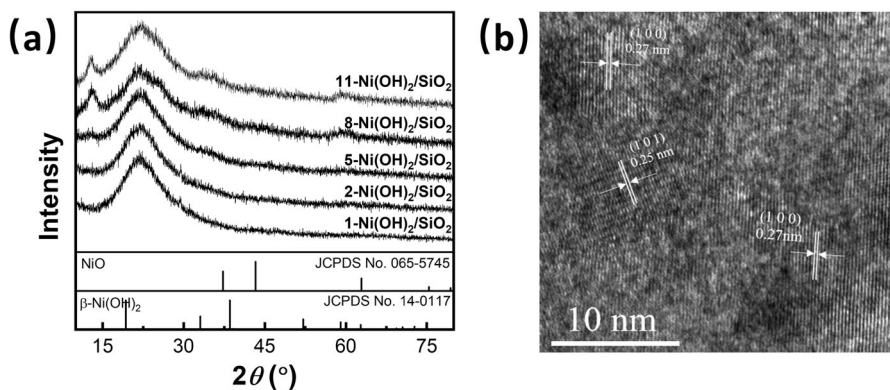

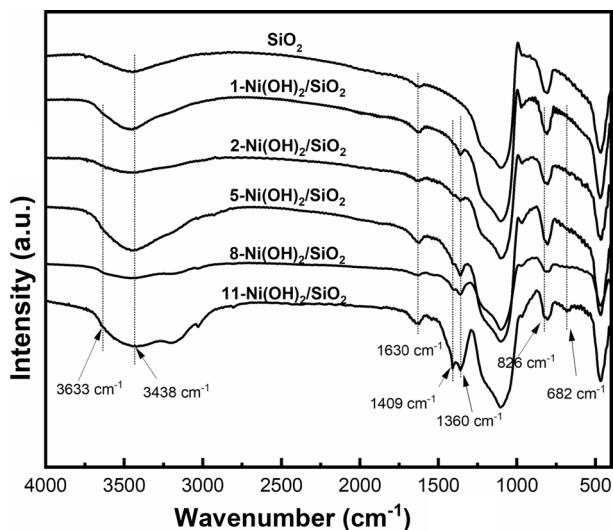**Fig. 1** XRD patterns for various α-Ni(OH)$_2$/SiO$_2$ catalysts (**a**) and HRTEM image of 5-Ni(OH)$_2$/SiO$_2$ (**b**)

Fig. 2 Infrared spectra for various α-Ni(OH)$_2$/SiO$_2$ catalysts

1630 cm^{-1} could be assigned to the the O–H bend from free H$_2$O [21]. Besides, an infrared absorption peak at about 1360 cm^{-1} and 826 cm^{-1} [20, 21] could be found in Fig. 2, which mainly was attributed to the intercalation of NO$_3^-$ in the layered structure of α-Ni(OH)$_2$. These results were in agreement with XRD analyses.

Whereafter, the XPS technique was conducted to identify the surface properties of the various α-Ni(OH)$_2$/SiO$_2$ catalysts. As shown in Fig. 3, the 2p levels of Ni^{2+}
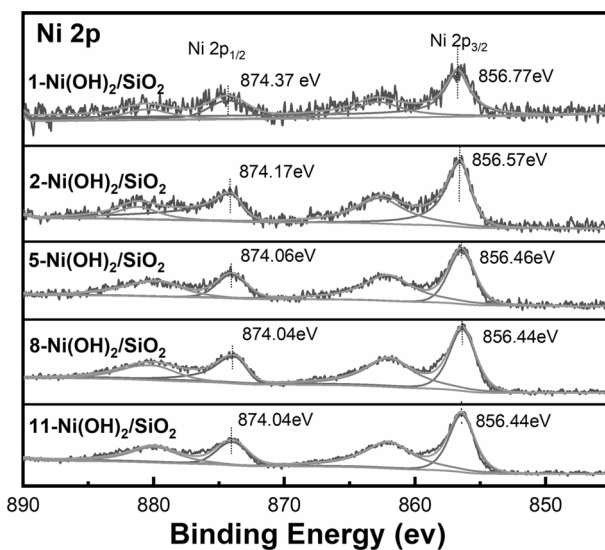
Fig. 3 XPS spectra of Ni 2p for various α-Ni(OH)$_2$/SiO$_2$ catalysts

were located at about 856 eV for $2p_{3/2}$ and about 874 eV for $2p_{1/2}$, which could be ascribed to the 2p levels of Ni^{2+} in $Ni(OH)_2$ [22, 23]. After careful comparison, the highest binding energy of 856.77 eV for Ni^{2+} 2p3/2 was found on the catalyst of 1-$Ni(OH)_2$/SiO_2. It might be due to the interaction between $Ni(OH)_2$ on the catalyst surface and the support of SiO_2. The electron shielding effect on Ni^{2+} would be strengthened by the strong interaction between $Ni(OH)_2$ and SiO_2 under the low Ni loading on the catalyst. With the increase of Ni loading, the size of $Ni(OH)_2$ would increase, the interaction between $Ni(OH)_2$ and SiO_2 might be weakened, and then the binding energy for the $2p_{3/2}$ levels of Ni^{2+} correspondingly decreased. The smaller binding energy of 856.46 eV for the $2p_{3/2}$ levels of Ni^{2+} would be found on the catalyst of 5-$Ni(OH)_2$/SiO_2. When the loading of Ni was greater than 5 wt%, the interaction of SiO_2 on $Ni(OH)_2$ on the catalyst surface might be negligible, which meant that the change of the binding energy for the $2p_{3/2}$ levels of Ni^{2+} could be ignored from the catalysts of 8-$Ni(OH)_2$/SiO_2 and 11-$Ni(OH)_2$/SiO_2.

H_2-TPR measurements were conducted over various α-$Ni(OH)_2$/SiO_2 catalysts. As shown in Fig. 4, the peak I at the range of 230 °C to 330 °C could be ascribed to the reduction of "α-$Ni(OH)_2$" to Ni^0 by one step [24, 25], while the α-$Ni(OH)_2$ would be decomposed to the NiO in this temperature range [26, 27]. Then, the NiO could be reduced to Ni^0 at the subsequent range of 330 °C to 500 °C of peak II [28–31]. Moreover, the peak III above 500 °C could be illustrated by the strong interaction of NiO with the –OH groups on the supports, and the difficultly reducible compound would be formed [29–31]. Intelligently, the stronger interaction between α-$Ni(OH)_2$ and SiO_2 would be found, when the smaller Ni loading was introduced on the SiO_2. Therefore, the hydrogen reduction peak I on the catalyst of 1-$Ni(OH)_2$/SiO_2 would locate at a high reduction temperature. With increasing the loading of Ni, the interaction between α-$Ni(OH)_2$ and SiO_2 might be weakened and lead to a lower reduction temperature for α-$Ni(OH)_2$ to Ni^0. However, the reduction temperature for α-$Ni(OH)_2$ to Ni^0 would be raised again for the larger crystal size of α-$Ni(OH)_2$, when the

Fig. 4 H$_2$-TPR profiles for various α-$Ni(OH)_2$/SiO_2 catalysts
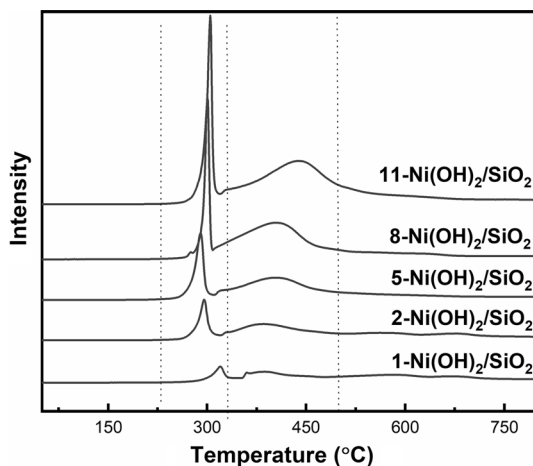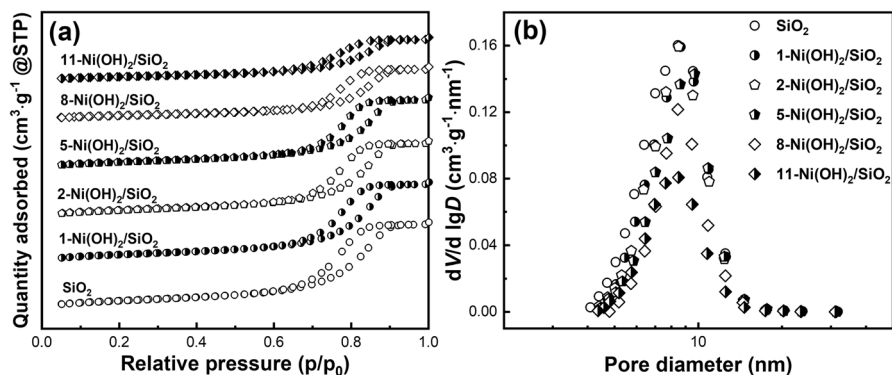
Fig. 5 N_2 adsorption–desorption isotherms (**a**) and pore-size distributions (**b**) of α-Ni(OH)$_2$/SiO$_2$ catalysts and SiO$_2$ support

Table 1 Properties of various α-Ni(OH)$_2$/SiO$_2$ catalysts

Catalysts	BET surface area (m² g⁻¹)	Pore volume (cm³ g⁻¹)	BJH average pore size (nm)	Ni content[a] (wt%)	Crystal size[b] (nm)
SiO$_2$	291.53	0.85	8.37	/	No detected
1-Ni(OH)$_2$/SiO$_2$	269.45	0.79	8.69	0.83	No detected
2-Ni(OH)$_2$/SiO$_2$	260.03	0.75	8.62	2.11	No detected
5-Ni(OH)$_2$/SiO$_2$	243.91	0.70	8.90	4.99	3.33
8-Ni(OH)$_2$/SiO$_2$	168.56	0.52	8.87	8.44	4.04
11-Ni(OH)$_2$/SiO$_2$	155.77	0.42	8.32	11.09	4.88

[a]Measured by ICP-OES technique

[b]Calculated by the Scherrer equation based on the XRD principal peak at 12.8°

Ni loading was large enough on the catalyst. A similar reduction behavior was also observed over the SiO$_2$-supported NiO species [30]. Based on the H$_2$-TPR results, the lowest reduced temperature of peak I could be found on the catalyst of 5-Ni(OH)$_2$/SiO$_2$ with about 5 wt% Ni, which might display the best performance on the hydrogenation of HMF.

Moreover, the N$_2$ adsorption–desorption analysis was performed on the catalysts for insight into the pore text of catalysts. As shown in Fig. 5. there is no significant change in the pore size distribution between the as-prepared catalysts with various Ni loading. After careful comparison, the pore size distribution of α-Ni(OH)$_2$/SiO$_2$ catalysts became very slightly larger than that of the support of SiO$_2$. This could be explained by the fact that the pores in SiO$_2$ are enlarged by ammonia corrosion under water vapor during the VIH treatment. Unlike the pore size distribution, an observable difference in specific surface area and pore volume could be obtained on the various catalysts which was shown in Table 1. It could be due to the pore blocking after Ni loading on SiO$_2$.

Reaction of HMF Hydrogenation over α-Ni(OH)$_2$/SiO$_2$ catalysts

The HMF hydrogenation was performed over the various α-Ni(OH)$_2$/SiO$_2$ catalysts without pre-reduction, and the results were plotted in Fig. 6. The conversion of HMF displayed a volcanic trend as a function of Ni content in the α-Ni(OH)$_2$/SiO$_2$ catalysts, and the highest HMF conversion of $87.6 \pm 5.0\%$ was achieved on the catalyst of 5-Ni(OH)$_2$/SiO$_2$ with about 5wt% Ni under the conditions of 195 °C and 0.2 MPa N$_2$ atmosphere for 5 h. This may be related to the interaction between the α-Ni(OH)$_2$ and the SiO$_2$ support, as well as the crystalline size of α-Ni(OH)$_2$. Generally, desirable interaction between the active component and the support as well as a reasonable crystalline size of the active component was favorable for the catalytic reaction. Moreover, the selectivity of BHMF gradually increased with the increase of Ni loading on the catalyst and was finally kept at about 84.3%. This could be attributed to the acidic Si–OH on the surface of SiO$_2$. Briefly, α-Ni(OH)$_2$ could not completely cover the surface of SiO$_2$ at a low Ni loading on the catalyst, and then the remaining Si–OH on the catalyst will stimulate the etherification reaction between BHMF and alcohols. As revealed in Scheme 1, two end−OH in the BHMF molecule will be further etherified with EtOH as the hydrogen donor in this work. Therefore, the EMFA and BEMF could be found in the mixture after the reaction. After prudential treatment, the intrinsic selectivity of BHMF could be calculated from the sum of the selectivities of BHMF, EMFA, and BEMF. Surprisingly, the intrinsic BHMF selectivity of about 98.9% was found over the α-Ni(OH)$_2$/SiO$_2$ catalysts, when the Ni loading in the catalyst was higher than 5 wt%. It also could be attributed to the acidic Si–OH on the surface of SiO$_2$. For comparison, an unsupported α-Ni(OH)$_2$
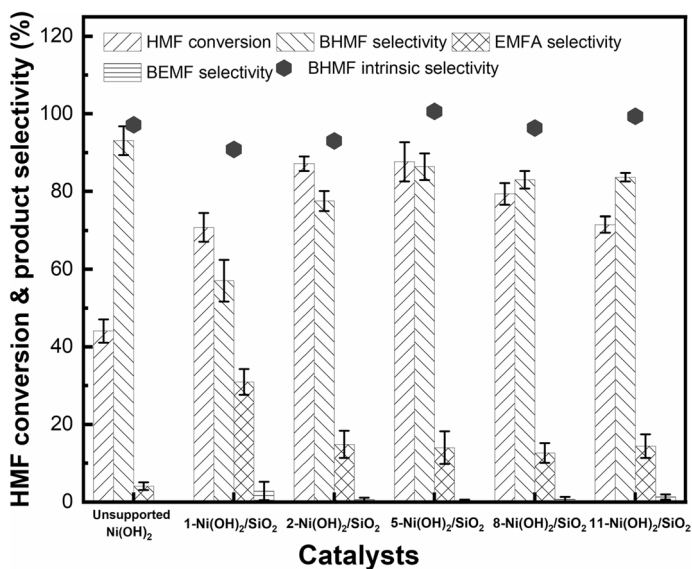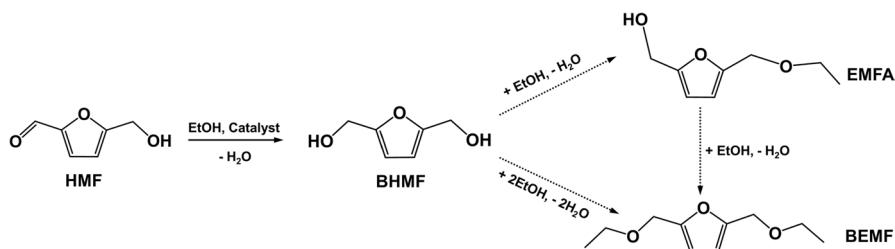

Fig. 6 HMF hydrogenation over various α-Ni(OH)$_2$/SiO$_2$ catalysts. (Reaction conditions: 195 °C, 0.5 mmol HMF in 30 mL EtOH, $n_{\text{Ni in catalyst}}$: $n_{\text{HMF}} = 1{:}10$ for 5 h)

Scheme 1 Plausible reaction pathway for the HMF Hydrogenation over α-Ni(OH)$_2$/SiO$_2$ catalyst

was prepared by using the VIH method and then was also applied to the HMF hydrogenation reaction. As shown in Fig. 6, about 44% HMF conversion was found on the unsupported α-Ni(OH)$_2$, which was not as good as that of the supported α-Ni(OH)$_2$/SiO$_2$. This could be due to insufficient dispersion of α-Ni(OH)$_2$ for the unsupported α-Ni(OH)$_2$. Noteworthily, a relatively high BHMF selectivity obtained on unsupported α-Ni(OH)$_2$ might be related to the absence of Si–OH.

Furthermore, the time course for the hydrogenation of HMF at 195 °C was examined to collect detailed information on the possible reaction pathway. As shown in Fig. 7a, the HMF conversion would be attached at about 100% after more than 7 h reaction. However, the selectivity of BHMF would decrease from 92.9% at the reaction time of 3 h to 69.3% at 11 h, and the etherification products of EMFA and BEMF formed from BHMF with EtOH would increase accordingly. Notable, the intrinsic selectivity of BHMF would decrease gradually for the generation of the unexpected byproducts. It could be due to the further hydrogenolysis or cracking of BHMF, EMFA, and BEMF for their larger diffusion resistance in the catalyst pore [32]. The influence of reaction temperature on the hydrogenation of HMF also was investigated on the α-Ni(OH)$_2$/SiO$_2$ catalysts, and the results were shown in Fig. 7b. It suggested that the reaction temperature was conducive to the increase in HMF conversion. However, side reactions such as degradation or polymerization would understandably be a favor to occur with the increase of reaction temperature. Understandingly, the selectivity of BHMF would decrease, which also could be found in Fig. 7b.
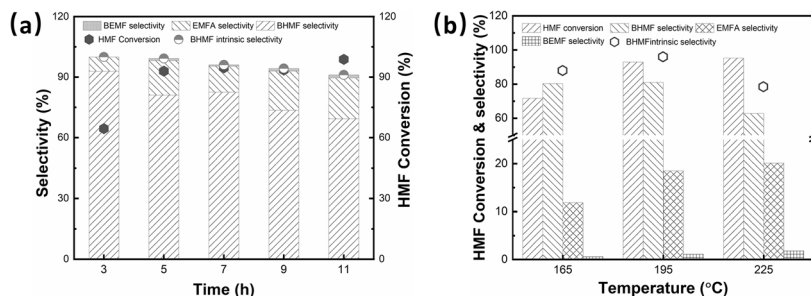

Fig. 7 Influence of (**a**) reaction time on HMF hydrogenation at 195 °C and (**b**) reaction temperature on HMF hydrogenation for 5 h on α-Ni(OH)$_2$/SiO$_2$ catalyst of 5-Ni(OH)$_2$/SiO$_2$

For insight into the recyclability of the α-Ni(OH)$_2$/SiO$_2$ catalyst, the recycling tests were performed on the 5-Ni(OH)$_2$/SiO$_2$ catalyst by successive reuse in this work. Before recycling, the used catalyst would be recovered by washing with ethanol, following dried at 110 °C for 1 h. Then, the next run test would be conducted on 5-Ni(OH)$_2$/SiO$_2$. Given the results in Fig. 8, the almost same HMF conversion of about 90% indicated that the catalyst was stable at its catalytic activity. In addition, no obvious distinction was found in the pore structure properties, XRD patterns, and XPS spectra between the fresh and recycled 5-Ni(OH)$_2$/SiO$_2$ in Fig. 9. This also understandably resulted in the activity stability of 5-Ni(OH)$_2$/SiO$_2$ at the HMF hydrogenation, which was in line with the results in Fig. 8. Notably, with the increase of the run number, although the intrinsic selectivity of BHMF almost kept unchanged, the selectivity of BHMF would decrease, and the selectivity of etherification products of EMFA and BEMF would increase accordingly. It might be related to the intercalated anions of NO$_3^-$ in "α-Ni(OH)$_2$ ". This electronegativity of NO$_3^-$ would be lost from the structure of "α-Ni(OH)$_2$ " when it undergoed the HMF hydrogenation with magnetic stirring. The evidence was shown in FT-IR spectra in Fig. 9d. It is found that the characteristic peaks at 1360 cm^{-1} and 826 cm^{-1} for NO$_3^-$ were obviously weakened after 4 cycles. These losing NO$_3^-$ increases the number of cationic Ni^{2+} with vacant coordination sites in "α-Ni(OH)$_2$ ", then it would play a role of Lewis acids. Generally, the presence of the acid will promote the etherification reaction. Surprisingly, the intrinsic BHMF selectivity was kept at almost the same, which could be found in Fig. 8. This almost constant intrinsic BHMF selectivity indirectly suggested the stability of catalyst activity. The BET surface area, pore volume, and BJH average pore size of the reused 5-Ni(OH)$_2$/SiO$_2$ were 263.87 m^2 g^{-1}, 0.72 cm^3 g^{-1}, and 8.37 nm, which were also not very significantly different from that of the fresh 5-Ni(OH)$_2$/SiO$_2$. Noteworthily, through an extremely careful
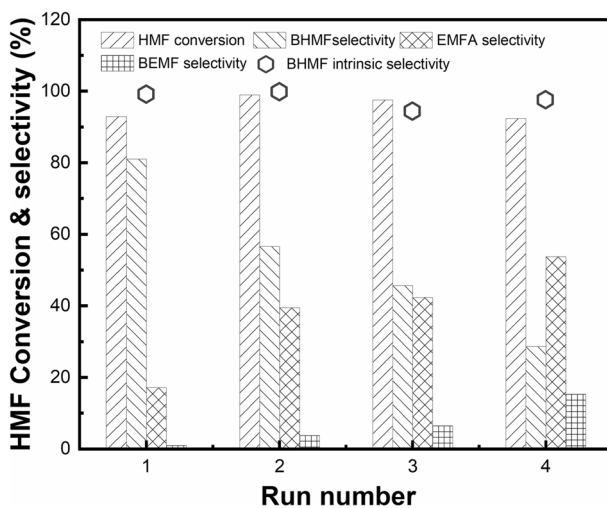

Fig. 8 Recyclability of α-Ni(OH)$_2$/SiO$_2$ catalyst of 5-Ni(OH)$_2$/SiO$_2$ for HMF hydrogenation at 195 °C for 5 h
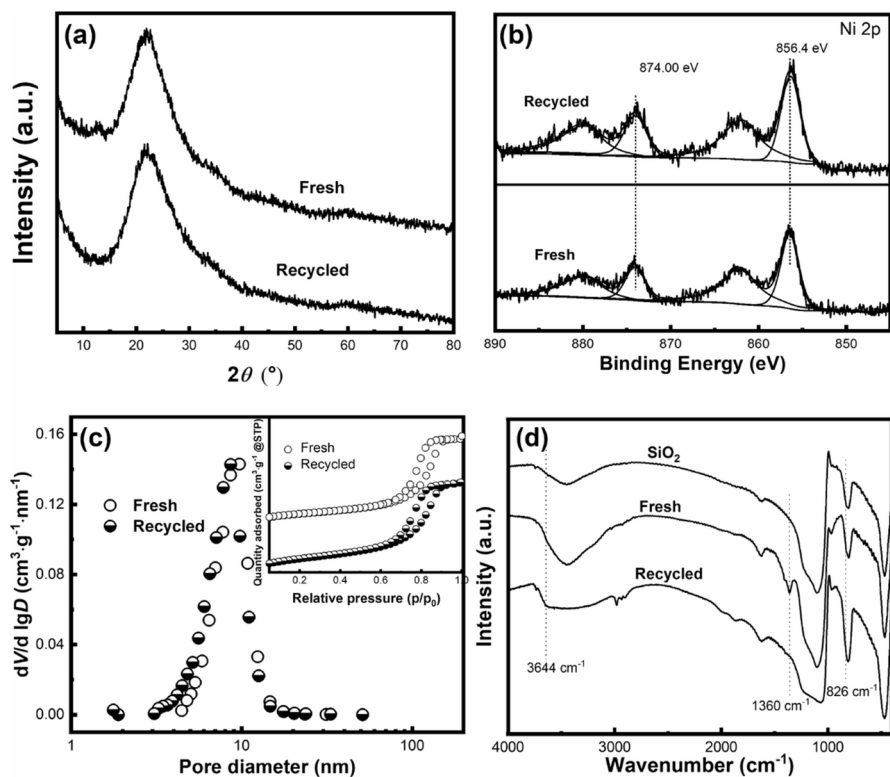
Fig. 9 XRD patterns (**a**), XPS spectra of Ni 2p (**b**), pore-size distributions (**c**), and FT-IR spectra (**d**) for the fresh and recycled α-Ni(OH)$_2$/SiO$_2$ catalyst of 5-Ni(OH)$_2$/SiO$_2$

comparison, a slight increase in the specific surface area for the reused catalyst could be found, which might be related to the loss of NO$_3^-$ from the interlayer in the α-Ni(OH)$_2$. Understandably, the hollow space would be formed after losing NO$_3^-$ from the interlayer in the α-Ni(OH)$_2$, thus the specific surface area of the used catalyst would correspondingly slightly increase in comparison with the fresh one.

Reaction mechanism of HMF Hydrogenation over α-Ni(OH)₂/SiO₂ catalyst

An integrated reaction mechanism over the α-Ni(OH)$_2$/SiO$_2$ catalysts was proposed in Scheme 2, which refers to the mechanism of Meerwein-Ponndorf-Verley (MPV) reaction. In this mechanism, the α-Ni(OH)$_2$ might play a key role during the HMF Hydrogenation. Firstly, the EtOH will easily attach at the −OH of α-Ni(OH)$_2$ for its alkalinity, and then nickel alkoxide I would form in Step 1. Secondly, a six-membered ring will be formed between HMF and the generated nickel alkoxide, then the acetaldehyde will be produced after transferring the α-H of the alkoxide to the C=O group via the six-membered ring transition. Subsequently, a new nickel alkoxide II will form in step 3 after releasing the acetaldehyde. Finally, an additional EtOH
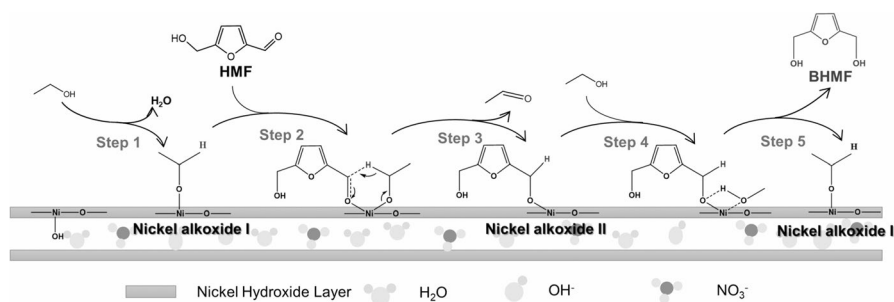
Scheme 2 Plausible reaction mechanism for the HMF Hydrogenation over α-Ni(OH)$_2$/SiO$_2$ catalyst

from the solution further coordinates with the nickel alkoxide II, and then the nickel alkoxide I will reform after releasing BHMF.

Conclusions

In this work, low-cost α-Ni(OH)$_2$/SiO$_2$ catalysts were successfully prepared by the vapor-induced internal hydrolysis method, which can exhibit superior catalytic performance for the HMF hydrogenation to BHMF without an extra pre-reduction treatment. The remarkable catalytic activity on the α-Ni(OH)$_2$/SiO$_2$ catalyst of 5-Ni(OH)$_2$/SiO$_2$ with about 5 wt% Ni was found that HMF conversion would be attached at about 87.6% with about 98.9% of the intrinsic selectivity of BHMF at 195 °C for 5 h under N$_2$ atmosphere and using the ethanol as the hydrogen donor. Based on the results from the recycling tests, the almost same HMF conversion and BHMF intrinsic selectivity were obtained, which could suggest that the catalyst was stable after four times of recycling.

Data Availability The data has been redescribed.

References

1. Tang X, Wei J, Ding N, Sun Y, Zeng X, Hu L, Liu S, Lei T, Lin L (2017) Chemoselective hydrogenation of biomass derived 5-hydroxymethylfurfural to diols: key intermediates for sustainable chemicals, materials and fuels. Renew Sust Energ Rev 77:287–296
2. Hameed S, Lin L, Wang A, Luo W (2020) Recent developments in metal-based catalysts for the catalytic aerobic oxidation of 5-hydroxymethyl-furfural to 2,5-furandicarboxylic acid. Catalysts 10(1):120

3. Fang W, Riisager A (2021) Recent advances in heterogeneous catalytic transfer hydrogenation/hydrogenolysis for valorization of biomass-derived furanic compounds. Green Chem 23(2):670–688

4. Wang L, Zuo J, Zhang Q, Peng F, Chen S, Liu Z (2022) Catalytic transfer hydrogenation of biomass-derived 5-hydroxymethylfurfural into 2,5-dihydroxymethylfuran over Co/UiO-66-NH$_2$. Catal Lett 152(2):361–371

5. Cao Q, Liang W, Guan J, Wang L, Qu Q, Zhang X, Wang X, Mu X (2014) Catalytic synthesis of 2,5-bis-methoxymethylfuran: a promising cetane number improver for diesel. Appl Catal A: Gen 481:49–53

6. Alipour S, Omidvarborna H, Kim DS (2017) A review on synthesis of alkoxymethyl furfural, a biofuel candidate. Renew Sust Energ Rev 71:908–926

7. Zhao W, Wang F, Zhao K, Liu X, Zhu X, Yan L, Yin Y, Xu Q, Yin D (2023) Recent advances in the catalytic production of bio-based diol 2,5-bis(hydroxymethyl)furan. Carbon Resources Convers 6(2):116–131

8. Alamillo R, Tucker M, Chia M, Pagán-Torres Y, Dumesic J (2012) The selective hydrogenation of biomass-derived 5-hydroxymethylfurfural using heterogeneous catalysts. Green Chem 14(5):1413–1419

9. Mishra DK, Lee HJ, Truong CC, Kim J, Suh Y-W, Baek J, Kim YJ (2020) Ru/MnCo$_2$O$_4$ as a catalyst for tunable synthesis of 2,5-bis(hydroxymethyl)furan or 2,5-bis(hydroxymethyl)tetrahydrofuran from hydrogenation of 5-hydroxymethylfurfural. Mol Catal 484:110722

10. Zhang K, Meng Q, Wu H, He M, Han B (2022) Selective hydrogenolysis of 5-hydroxymethylfurfural into 2,5-dimethylfuran under mild conditions using Pd/MOF-808. ACS Sustain Chem Eng 10(31):10286–10293

11. Padilla R, Koranchalil S, Nielsen M (2020) Efficient and selective catalytic hydrogenation of furanic aldehydes using well defined Ru and Ir pincer complexes. Green Chem 22(20):6767–6772

12. Hao W, Li W, Tang X, Zeng X, Sun Y, Liu S, Lin L (2016) Catalytic transfer hydrogenation of biomass-derived 5-hydroxymethyl furfural to the building block 2,5-bishydroxymethyl furan. Green Chem 18(4):1080–1088

13. Valentini F, Kozell V, Petrucci C, Marrocchi A, Gu Y, Gelman D, Vaccaro L (2019) Formic acid, a biomass-derived source of energy and hydrogen for biomass upgrading. Energ Environ Sci 12(9):2646–2664

14. Johnson TC, Morris DJ, Wills M (2010) Hydrogen generation from formic acid and alcohols using homogeneous catalysts. Chem Soc Rev 39(1):81–88

15. Krishnan CK, Hayashi T, Ogura M (2008) A new method for post-synthesis coating of zirconia on the mesopore walls of SBA-15 without pore blocking. Adv Mater 20(11):2131–2136

16. Wallbridge SP, Lawson K, Catling AE, Kirk CA, Dann SE (2022) Synthesis and spectroscopic identification of nickel and cobalt layered hydroxides and hydroxynitrates. Dalton T 51(47):18010–18023

17. Xu L, Ding Y-S, Chen C-H, Zhao L, Rimkus C, Joesten R, Suib SL (2008) 3D flowerlike α-nickel hydroxide with enhanced electrochemical activity aynthesized by microwave-assisted hydrothermal method. Chem Mater 20(1):308–316

18. Rajamathi M, Vishnu Kamath P (1998) On the relationship between α-nickel hydroxide and the basic salts of nickel. J Power Sources 70(1):118–121

19. Ma Y, Yang M, Jin X (2020) Formation mechanisms for hierarchical nickel hydroxide microstructures hydrothermally prepared with different nickel salt precursors. Coll Surface A 588:124374

20. Park S, Khan Z, Shin TJ, Kim Y, Ko H (2019) Rechargeable Na/Ni batteries based on the Ni(OH)$_2$/NiOOH redox couple with high energy density and good cycling performance. J Mater Chem A 7(4):1564–1573

21. Hall DS, Lockwood DJ, Poirier S, Bock C, MacDougall BR (2012) Raman and infrared spectroscopy of α and β phases of thin nickel hydroxide films electrochemically formed on nickel. J Phys Chem A 116(25):6771–6784

22. Xa C, Chen X, Zhang F, Yang Z, Huang S (2013) One-pot hydrothermal synthesis of reduced graphene oxide/carbon nanotube/α-Ni(OH)$_2$ composites for high performance electrochemical supercapacitor. J Power Source 243:555–561

23. Grosseau-Poussard JL, Dinhut JF, Silvain JF, Sabot R (1999) Role of a chromium ion implantation on the corrosion behaviour of nickel in artificial sea water. Appl Surface Sci 151(1):49–62

24. Ghesquiere C, Lemaitre J, Herbillon AJ (1982) An investigation of the nature and reducibility of Ni-hydroxy-montmorillonites using various methods including temperature-programmed reduction (TPR). Clay Miner 17(2):217–230

25. Wang CB, Gau GY, Gau SJ, Tang CW, Bi JL (2005) Preparation and characterization of nanosized nickel oxide. Catal Lett 101(3):241–247
26. Aghazadeh M, Golikand AN, Ghaemi M (2011) Synthesis, characterization, and electrochemical properties of ultrafine β-Ni(OH)$_2$ nanoparticles. Int J Hydrogen Energ 36(14):8674–8679
27. Baraldi P, Davolio G, Fabbri G, Manfredini T (1989) A spectral and thermal study on nickel(II) hydroxydes. Mater Chem Phys 21(5):479–493
28. Clause O, Bonneviot L, Che M (1992) Effect of the preparation method on the thermal stability of silica-supported nickel oxide as studied by EXAFS and TPR techniques. J Catal 138(1):195–205
29. Zhang C, Zhu W, Li S, Wu G, Ma X, Wang X, Gong J (2013) Sintering-resistant Ni-based reforming catalysts obtained via the nanoconfinement effect. Chem Commun 49(82):9383–9385
30. Zhang X, Tang W, Zhang Q, Wang T, Ma L (2017) Hydrocarbons production from lignin-derived phenolic compounds over Ni/SiO$_2$ catalyst. Energy Procedia 105:518–523
31. Xia WS, Hou YH, Chang G, Weng WZ, Han GB, Wan HL (2012) Partial oxidation of methane into syngas (H$_2$+CO) over effective high-dispersed Ni/SiO$_2$ catalysts synthesized by a sol-gel method. Int J Hydrogen Energ 37(10):8343–8353
32. Hu D, Hu H, Jin H, Zhang P, Hu Y, Ying S, Li X, Yang Y, Zhang J, Wang L (2020) Building hierarchical zeolite structure by post-synthesis treatment to promote the conversion of furanic molecules into biofuels. Appl Catal A: Gen 590:117338